

## Full length article

# A poly(L-glutamic acid)-combretastatin A4 conjugate for solid tumor therapy: Markedly improved therapeutic efficiency through its low tissue penetration in solid tumor



Tianzhou Liu<sup>a</sup>, Dawei Zhang<sup>c</sup>, Wantong Song<sup>c</sup>, Zhaohui Tang<sup>c,\*</sup>, Jiaming Zhu<sup>a</sup>, Zhiming Ma<sup>a</sup>, Xudong Wang<sup>a</sup>, Xuesi Chen<sup>c</sup>, Ti Tong<sup>b,\*</sup>

<sup>a</sup> Department of Gastrointestinal Surgery, The Second Hospital of Jilin University, Changchun 130041, PR China

<sup>b</sup> Department of Thoracic Surgery, The Second Hospital of Jilin University, Changchun 130041, PR China

<sup>c</sup> Key Laboratory of Polymer Ecomaterials, Changchun Institute of Applied Chemistry, Chinese Academy of Sciences, Changchun 130022, PR China

## ARTICLE INFO

## Article history:

Received 1 September 2016

Received in revised form 30 January 2017

Accepted 1 February 2017

Available online 3 February 2017

## Keywords:

Vascular disrupting agents

Combretastatin A4

Nanomedicine

Tumor therapy

Delivery

Glutamic acid

## ABSTRACT

Combretastatin A4 (CA4) is a leading agent in vascular disrupting strategies for tumor therapy. Although many small-molecule prodrugs of CA4 have been developed to improve its solubility, the overall therapeutic efficiency is moderate. A key reason for this is the reversible effect that CA4 has on tubulin as well as its rapid clearance from plasma and tissues. In this study, we proposed a poly(L-glutamic acid)-CA4 conjugate (PLG-CA4) nanomedicine to fulfill the requirements for fully liberating the potential of CA4 on tumor therapy. Enhanced accumulation and retention of CA4 in tumor tissue, especially, high distribution and gradual release around tumor blood vessels resulted in prolonged vascular disruption and markedly enhanced therapeutic efficiency. We examined and compared the therapeutic effect of PLG-CA4 and commercial combretastatin-A4 phosphate (CA4P) in a murine colon C26 tumor. PLG-CA4 showed significantly prolonged retention in plasma and tumor tissue. Most importantly, the PLG-CA4 was mainly distributed around the tumor vessels because of its low tissue penetration in solid tumor. Pathology tests showed that PLG-CA4 treatment resulted in persistent vascular disruption and tumor damage 72 h after a single injection, this in contrast to CA4P treatment, which showed quick relapse at an equal dose. Tumor suppression tests showed that PLG-CA4 treatment resulted in a tumor suppression rate of 74%, which indicates a significant advantage when compared to tumor suppression rate of the CA4P group, which was 24%. This is the first time that an advantage of the polymeric CA4 nanomedicine with low tissue penetration for solid tumor therapy has been shown. Thus, the results presented in this study provide a new idea for enhancing the tumor therapeutic effect of vascular disrupting agents.

## Statement of Significance

Nanomedicine usually has low tissue penetration in solid tumors, which limits the efficacy of nanomedicine in most cases. But herein, we demonstrate a nanosized vascular disruptive agent (VDA) PLG-CA4 has superior advantages over small molecular combretastatin-A4 phosphate (CA4P) because the PLG-CA4 was mainly distributed around the tumor vessels due to its low tissue penetration in solid tumor.

© 2017 Acta Materialia Inc. Published by Elsevier Ltd. All rights reserved.

## 1. Introduction

The tumor vasculature is an attractive target for tumor therapy [1–3]. It has been reported that when tumors grow to a size larger than 2–3 mm<sup>3</sup>, their continued proliferation strongly depends on angiogenesis [4–6]. As a result, various drugs targeting tumor-

initiated angiogenic processes or destroying the established tumor vessel network (angiogenesis inhibitors (AIs) and vascular disrupting agents (VDAs) respectively), have been developed and are currently under clinical evaluation [7,8].

VDAs cause a rapid and selective vascular shutdown in tumors to produce extensive secondary neoplastic cell death due to ischemia [9–11]. CA4 is a lead agent in VDAs. As a microtubule depolymerizing agent, CA4 binds at or near the colchicine binding site of  $\beta$ -tubulin, which leads to cytoskeletal and morphological changes

\* Corresponding authors.

E-mail addresses: [ztang@ciac.ac.cn](mailto:ztang@ciac.ac.cn) (Z. Tang), [titong2012@163.com](mailto:titong2012@163.com) (T. Tong).

in endothelial cells [12,13]. These changes increase vascular permeability, disrupt tumor blood flow, and rapidly lead to widespread ischemic necrosis [2,14,15]. Studies have shown that CA4 has dramatic effects on the three-dimensional shape of newly formed endothelial cells, with little or no effect on quiescent endothelial cells [16]. In addition, CA4 has been demonstrated to disrupt cell-cell contacts between endothelial cells mediated by vascular endothelial (VE)-cadherin/ $\beta$ -catenin complexes and this effect could be inhibited in the presence of smooth muscle cells [17]. Since tumor blood vessels are characterized by recently formed endothelial cells and abnormal vessels that lack a full complement of smooth muscle or pericyte support, CA4 shows selective vascular damage in tumor tissues.

Because of its insolubility in water, CA4 cannot directly be intravenously administered. In recent years, various small-molecule prodrug derivatives of CA4 have been developed [18,19]. Of these, CA4 phosphate (CA4P) is the leading agent [20]. Phosphate greatly improved the solubility of CA4, and is able to release CA4 in the presence of phosphoesterase [21]. Clinical studies of CA4P consist of 18 completed and ongoing clinical trials in oncology and ophthalmology [22]. Overall, CA4P monotherapy was well tolerated, with most adverse events being of mild to moderate intensity [23–25]. In a phase II clinical trial in which CA4P was used to treat anaplastic thyroid cancer (ATC), the median survival was 4.7 months of which 34% of patients were alive at 6 months and 23% of patients was alive at 12 months. Median duration of stable disease in seven patients was 12.3 months (4.4–37.9 months). However, there were no objective responses observed after single-agent CA4P administration in this trial and the primary endpoint of survival doubling was not observed [26]. As a result, phase III clinical trials of CA4P on ATC were conducted as a combination therapy using CA4P with carboplatin/paclitaxel.

The limited therapeutic efficacy of small-molecule prodrug derivatives of CA4 lies in the reversible effects CA4 has on tubulin as well as its rapid clearance from plasma and tissues. Unlike changes induced by colchicines and vinblastine the changes in endothelial cell shape induced by CA4 can be reversed after drug removal [16]. CA4 rapidly binds to tubulin and dissociates from tubulin over 100 times faster than colchicines. At 37 °C, CA4 half-life is 3.6 min compared to 405 min for colchicines [27]. Moreover, these small-molecule drugs have a relatively short half-life *in vivo*. In phase I clinical trials, the distribution half-life time ( $t_{1/2\alpha}$ ) of CA4P is 0.103 h and the elimination half-life time ( $t_{1/2\beta}$ ) is 0.489 h [25]. As a result, the tentatively closed tumor vascular can recover and continuously provide oxygen and nutrients and nutrients for tumor growth. Therefore, single administration of small-molecule prodrug derivatives of CA4 may not significantly affect primary tumor growth [28,29].

A key point in improving the therapeutic efficacy of CA4 is to keep a constant concentration around the endothelial cells and enhance the action time on tubulin. Nanocarrier-based drug delivery systems provide an ideal medium to realize this. Nanocarrier-encapsulated or -conjugated drugs have been extensively examined for prolonging the retention time of small-molecule drugs *in vivo*, and increasing drug accumulation in the tumor tissue by virtue of the “enhanced permeability and retention” (EPR) effect [30–35]. This system allows for gradual or temporary release of free active drugs from the nanocarriers in a controlled fashion, and allows for a constant drug concentration in the tumor tissue [36–38]. More importantly, because of the high interstitial pressure and low diffusion efficiency inside solid tumors, nanocarrier-loaded drugs are frequently observed around blood vessels in solid tumors because of the low tissue penetration [39–43]. We consider these characteristics are especially important to improve the efficiency of CA4 treatment in tumor therapy, since the action target of CA4 are endothelial cells of

tumor blood vessels. Therefore, a nanocarrier-loaded CA4 prodrug is expected to enhance CA4 accumulation and retention in the tumor tissue, high distribution and gradual release CA4 around tumor blood vessels, resulting in prolonged vascular disruption and markedly enhanced tumor therapeutic efficacy.

In this study, we proposed to derive a poly(L-glutamic acid)-CA4 (PLG-CA4) conjugate nanomedicine to examine the effect of polymeric design on CA4 efficacy. The following studies were conducted: 1) Preparation and characterization of PLG-CA4, 2) pharmacokinetics of PLG-CA4, 3) multispectral optoacoustic tomography (MSOT) and immunofluorescence analysis of PLG-CA4 distribution inside tumors, 4) pathological response of murine C26 tumors to PLG-CA4 and CA4P treatment, 5) tumor therapy tests. In summary, we found that nanosized polymeric CA4 prodrugs have advantages over small-molecule CA4 prodrugs.

## 2. Experimental

### 2.1. Materials

$\gamma$ -Benzyl-L-glutamate-N-carboxyanhydride (BLG-NCA) was purchased from Chengdu Enlai Biological Technology CO., Ltd., China. mPEG5k and 4',6'-diamidino-2-phenylindole dihydrochloride (DAPI) was purchased from Sigma-Aldrich, USA. Combretastatin A4 (CA4) and combretastatin-A4 phosphate (CA4P) were purchased from Hangzhou Great Forest Biomedical Ltd., China. 2,4,6-trichlorobenzoyl chloride, 4-dimethylaminopyridine (DMAP), 1-ethyl-3-(3-dimethylaminopropyl)-carbodiimide hydrochloride (EDC-HCl) and N-hydroxysuccinimide (NHS) were supplied by Aladdin Reagent Co. Ltd, China. Rhodamine B-NH<sub>2</sub> (RhoB-NH<sub>2</sub>) was a kind gift from Dr. Chunsheng Xiao, Changchun Institute of Applied Chemistry, Chinese Academy of Sciences. Anti-mouse, human and pig CD31 antibody (ab28364) was purchased from Abcam, USA. All other reagents and solvents were purchased from Sinopharm Chemical Reagent Co., Ltd, China.

### 2.2. Preparation and characterization of PLG-CA4

Poly(L-glutamic acid)-graft-methoxy poly(ethylene glycol) copolymer (PLG-g-mPEG) was prepared as described previously [43–45]. PLG-g-mPEG has an average of 160 L-glutamic acid repeating units and an average of 8.3 mPEG5k chains. The number-average molecular weight ( $M_n$ ) and molecular weight distribution (PDI) of the PLG-g-mPEG (Determined by GPC using PEG as standards and phosphate buffer pH 7.4 as eluent) were  $37.3 \times 10^3 \text{ g mol}^{-1}$  and 1.91, respectively [44]. CA4 was grafted to PLG-g-mPEG by the Yamaguchi reaction. Briefly, PLG-g-mPEG (585 mg) was dissolved in 10 mL anhydrous N,N-dimethylformamide (DMF) in a glass reactor, then CA4 (1.0 mmol, 316 mg), 2,4,6-trichlorobenzoyl chloride (1.1 mmol, 268 mg), DMAP (1.1 mmol, 135 mg) and triethylamine (1.1 mmol, 111 mg) were dissolved in 5 mL anhydrous DMF and added to the above mixture. The reaction was allowed to proceed at room temperature for 2 h. After that, the reaction mixture was precipitated into excess diethyl ether, re-dissolved in DMF, and dialyzed against distilled water (MWCO 3500). The final product poly(L-glutamic acid)-graft-methoxy poly(ethylene glycol)/combretastatin A4 (PLG-CA4) was obtained after lyophilization.

Chemical structure of the synthesized PLG-CA4 was confirmed by <sup>1</sup>H NMR (D<sub>2</sub>O, Bruker AV 400 NMR spectrometer).  $M_n$  ( $57.3 \times 10^3 \text{ g mol}^{-1}$ ) and PDI (1.69) of the PLG-CA4 were determined by gel permeation chromatography (GPC, Waters 515 pump, 2414 detector, DMF containing 0.01 M LiBr as the eluent and using polystyrene as standard samples). Free CA4 contents were measured using a high-performance liquid chromatography

(HPLC) system, containing a reverse-phase C18 column, UV-Vis detector at 305 nm, with a mobile phase of acetonitrile and water (80/20, v/v) pumped at a flow rate of 1.0 mL/min. The hydrodynamic diameter ( $D_h$ ) of PLG-CA4 dispersed in PBS (pH 7.4) was determined by dynamic laser scattering (DLS), on a Brookhaven ZetaPlus Analyzer (Brookhaven Instrument, USA) with a 90° scatter angle. Transmission electron microscopy (TEM) images were taken on a JEOL FEM-1011 transmission electron microscope at an accelerating voltage of 100 kV. CA4 loading content was calculated by measuring the UV-Vis absorbance at 290 nm in DMF/H<sub>2</sub>O (v/v = 1/1). The drug loading content (DLC%) was calculated using the following formulation:

$$\text{DLC\%} = (\text{weight of loaded drug/weight of micelles}) \times 100\%$$

IR830-labeled PLG-CA4 and RhoB-labeled PLG-CA4 were prepared in a similar fashion as described previously [39,46]. The maximum absorbance of IR830-labeled PLG-CA4 in water is 815 nm, and the maximum absorbance of RhoB-labeled PLG-CA4 in water is 563 nm.

### 2.3. *In vitro* release profiles

*In vitro* release of CA4 from PLG-CA4 was conducted using a dialysis method. Briefly, 3.0 mg PLG-CA4 was dissolved in 5 mL distilled water, PBS solution at pH 7.4 or 5.5, respectively. Samples were sealed in a dialysis bag (MWCO 3500 Da) and incubated in 45 mL of PBS at 37 °C with a shaking rate of 100 rpm. At predetermined time points (1, 2, 4, 8, 24, 36, 48 h), 3 mL of the incubated solution was taken out and replaced with fresh media. The concentration of CA4 in the released media was determined by HPLC at 305 nm with a mobile phase of acetonitrile and water (80/20, v/v), as described above.

### 2.4. Cell culture and animal use

C26 murine colon carcinoma cells were purchased from Shanghai Bogoo Biotechnology Co. Ltd., China. Cells were cultured in complete Dulbecco's modified Eagle's medium (DMEM) containing 10% fetal bovine serum, supplemented with 50 U/mL penicillin and 50 U/mL streptomycin, and incubated at 37 °C in a 5% CO<sub>2</sub> atmosphere. Balb/C mice were obtained from the Laboratory Animal Center of Jilin University. Balb/C nude mice and Wistar rats were obtained from Beijing Huafukang Biological Technology Co. Ltd. (HFK Bioscience, Beijing). The C26 xenograft tumor model was prepared by injecting  $2.0 \times 10^6$  C26 cells into the right flank of male Balb/C or Balb/C nude mice. All animal experiments were conducted in accordance with the guidelines of the Laboratory Protocol of Animal Care and Use Committee, Jilin University.

### 2.5. *In vitro* tumor cell inhibition test

#### 2.5.1. Cell viability assay

C26 cells were seeded in 96-well plates at a density of 7000 cells per well in 200  $\mu$ L DMEM. After 24 h, the culture medium was removed and replaced with medium containing CA4P or PLG-CA4 at different concentrations. After incubating for 24 or 48 h, the cells were subjected to MTT assay, and absorbance was measured using a Bio-Rad 680 microplate reader at 492 nm. Cell viability was calculated according to the following equation:

$$\text{viability (\%)} = (A_{\text{sample}}/A_{\text{control}}) \times 100\%$$

where  $A_{\text{sample}}$  and  $A_{\text{control}}$  are absorbances of the sample and control wells, respectively.

#### 2.5.2. Cell growth assay

C26 cells were seeded in 96-well plates at a density of 4000 cells per well in 200  $\mu$ L DMEM. The cells were incubated overnight. The culture medium was removed and replaced with 100  $\mu$ L medium containing CA4P or PLG-CA4 (50  $\mu$ g/mL on the basis of CA4). After 3, 6, 24 or 48 h incubation, CCK-8 (Dojindo Laboratories, Kumamoto, Japan) solution (10  $\mu$ L) was added to each well, and the cells were incubated for an additional 2 h. The number of cell was counted by measuring the absorbance at 450 nm using a microplate reader.

### 2.6. Pharmacokinetics

For PLG-CA4, Wistar rats ( $n = 3$ , male, average body weight 250 g) were administered with PLG-CA4 *via* tail vein at a dose of 50.0 mg/kg on the basis of CA4. At defined time points (5 min, 20 min, 40 min, 1 h, 2 h, 4 h, 8 h, 12 h, and 24 h), blood samples were collected from the orbital cavity, heparinized, and centrifuged to obtain plasma. For each of the samples, 50  $\mu$ L plasma was added to 100  $\mu$ L 1 N NaOH, then hydrolyzed at 60 °C for 4 h. H<sub>3</sub>PO<sub>4</sub> (1.4 mol/L 50  $\mu$ L) was added. After 30 min of reaction, 400  $\mu$ L MeOH was added and the mixture was vortexed and centrifuged. The extracts were passed through a 0.22  $\mu$ m filter and the total CA4 concentrations were determined using a HPLC system, in a similar fashion as described above.

For CA4P, Wistar rats ( $n = 3$ , male, average body weight 250 g) were administered with CA4P *via* tail vein at a dose of 50.0 mg/kg on the basis of CA4. At defined time points (0.05, 0.5, 1, 2, 4, 5, 6, 7 and 8 h), blood samples were collected from the orbital cavity, heparinized, and centrifuged to obtain plasma. For each of the samples, 50  $\mu$ L plasma was added to 500  $\mu$ L MeOH, then the mixture was vortexed and centrifuged. The extracts were passed through a 0.22  $\mu$ m filter and free CA4 concentrations were determined using a HPLC system, in a similar fashion as described above. CA4P concentrations were measured using a high-performance liquid chromatography (HPLC) system, containing a reverse-phase C18 column, UV-Vis detector at 295 nm, with eluents: A: 5 mM KH<sub>2</sub>PO<sub>4</sub>, 5 mM H<sub>3</sub>PO<sub>4</sub>; B: 75 % acetonitrile, 25% water; gradient 40–85% B in 5 min. The total CA4 concentration was calculated from released CA4 concentration plus CA4P concentration (on the basis of CA4).

### 2.7. Free CA4 in tumor after the administration of CA4P or PLG-CA4

Balb/C mice bearing C26 tumors of a volume of approximately 200 mm<sup>3</sup> were prepared similarly as described in the methods section above. Mice were divided into 6 groups (4 mice per group), injected with CA4P or PLG-CA4 *via* tail vein at a CA4 dose of 50.0 mg/kg. At predetermined time points (1, 4 and 24 h), mice were sacrificed but not exsanguinated. The tumors were collected and homogenized in H<sub>2</sub>O/MeOH and centrifuged. The extracts were passed through a 0.22  $\mu$ m filter and free CA4 concentrations were determined using a HPLC system, as described above.

### 2.8. Multispectral optoacoustic tomography imaging

The MSOT equipment (inVision 128) was from iThera Medical (Munich, Germany). Balb/C nude mice bearing C26 tumors at a volume of approximately 200 mm<sup>3</sup> were injected *via* tail vein with IR830-labeled PLG-CA4 at a dose of 136 mg/kg (50.0 mg/kg on the basis of CA4). The mice were imaged at different time points (0, 4, 24, 48 and 72 h). At each time point, the mice were anaesthetized with 2% isoflurane and placed into the MSOT system. Multispectral process (MSP) scanning was performed at 680 nm, 715 nm, 730 nm, 760 nm, 815 nm, 850 nm and 900 nm. The results

were reconstructed in a linear model and analyzed via linear regression.

### 2.9. Ex vivo RhoB-labeled PLG-CA4 fluorescence imaging

The RhoB-labeled PLG-CA4 (50 mg/kg on CA4 basis) and saline were injected into mice bearing C26 tumor via lateral tail vein. The mice were sacrificed 4 and 24 h post-injection. The tumor and major organs (heart, liver, spleen, lung, and kidney) were excised, followed by washing the surface with physiological saline three times for ex vivo imaging of Rhodamine B fluorescence using the Maestro *in vivo* Imaging System (Cambridge Research & Instrumentation, Inc., USA). The resulting data can be used to identify, separate, and remove the contribution of autofluorescence in analyzed images by the commercial software (Maestro 2.4). The average signals were also quantitatively analyzed using Maestro 2.4 software.

### 2.10. Immunohistochemical staining of tumor tissue

Balb/C mice bearing C26 tumors at volume of about 200 mm<sup>3</sup> were injected with RhoB-labeled PLG-CA4 via tail vein at a CA4 dose of 50.0 mg/kg. After 24 h, the mice were sacrificed and tumors were collected, frozen and sectioned (5 μm in thickness) using a microtome (Leica CM 1900).

Immunohistochemical staining was carried out following the immunocytochemistry (ICC) protocol provided by Abcam. Briefly, sections were fixed in 4% paraformaldehyde at room temperature for 15 min, washed three times with PBS, and incubated with 1% BSA in phosphate buffered saline Tween-20 (PBST) for 30 min to block unspecific binding of antibodies. Next, sections were incubated with an anti-CD31 antibody (1:50 diluted in 1% BSA in PBST) in a humidified chamber for 1 h at 37 °C, followed by incubation with a secondary antibody (FITC-labeled goat anti-rabbit IgG) in PBST for 1 h at 37 °C in the dark. After extensive washing with PBS, sections were counterstained with DAPI for 1 min, and images were taken under a confocal laser scanning microscope (CLSM, Carl Zeiss LSM 780).

### 2.11. Hematoxylin and eosin staining

For comparison purposes, Balb/C mice bearing C26 tumors at volume of about 200 mm<sup>3</sup> were divided into two groups (4 mice per group) and injected with CA4P or PLG-CA4 at a CA4 dose of 50.0 mg/kg. The mice were sacrificed at different time points (4, 24, 48 and 72 h). Tumors were fixed in 10% formalin (Sigma, St. Louis, MO), embedded in paraffin, sectioned at 4 μm thickness and stained by haematoxylin and eosin (H&E). Histological images were taken under a microscope (Nikon TI-S/L100) and images were analyzed using ImageJ software (NIH, Bethesda, MD, USA).

### 2.12. Vessel density

An immunohistochemical assay for CD31 was performed to analyze whole tumor vessel density [47–49]. Balb/C mice bearing C26 tumors at volume of about 200 mm<sup>3</sup> were divided into three groups ( $n = 4$  per group) and injected with saline, CA4P or PLG-CA4 at a CA4 dose of 50.0 mg/kg. Mice were sacrificed at different time points (1, 4, 24, 48 and 72 h) and tumors were collected, sectioned and fixed in a 1:1 solution of acetone and methanol. Sections were blocked in 5% horse and 1% goat serum in PBS with 0.1% Tween-20, and incubated with an anti-CD31 antibody conjugated with R-Phycoerythrin (R-PE) overnight at 4 °C (Southern Biotech, Birmingham, AL). The CD31 staining sections were first scanned at a low magnification, and the areas with the greatest density of positively stained vessels (“hot spots”) were selected

for further evaluation. The microvessel count was then determined by counting all immunostained vessels in 3 representative hot spots at 100× magnification, with each section being counted twice. The tumor vessel density in the 3 selected vessel hot spots was then calculated.

### 2.13. In vivo tumor therapy

The therapeutic efficacy of CA4P and PLG-CA4 treatment was evaluated utilizing Balb/C mice bearing C26 tumors. After tumors reached approximately 100 mm<sup>3</sup>, the mice were weighed, randomly divided into three groups (6 mice per group) and treated with saline, CA4P and PLG-CA4 at a CA4 dose of 50.0 mg/kg. Injections were carried out on days 1, 5 and 9 via tail vein. Treatment efficacy and safety profiles were evaluated by measuring the tumor volumes and body weight changes. Photographs of mice bearing tumors were taken on day 11. Tumor volume ( $V_t$ ) and tumor suppression rate (TSR%) were calculated as follows:

$V_t = a \times b^2/2$ , where  $a$  is the major axis and  $b$  is the minor axis of the tumor.

$TSR\% = [(V_c - V_x)/V_c] \times 100\%$ , where  $V_c$  represents the average tumor volume of the control group and  $V_x$  represents the average tumor volume of the treatment group.

### 2.14. Statistical analysis

Values represent mean ± SD and were determined by Student's  $t$  test.  $P$  values of <0.05 were considered significant.

## 3. Results and discussion

### 3.1. Preparation and characterization of PLG-CA4

Poly(L-glutamic acid) (PLG)-based polymeric-drug conjugates have consistently been used for drug development. PLG is biocompatible, biodegradable, and can be easily modified [50–54]. As a drug conjugate, PLG is linked to various small molecular drugs such as cisplatin (CDDP), paclitaxel (PTX) and camptothecin (CPT) to improve its longevity and bioavailability [55–58]. In this study, CA4 was conjugated to PLG-g-mPEG using a one-step Yamaguchi reaction catalyzed by 2,4,6-trichlorobenzoyl chloride and DMAP (Fig. 1A). The chemical structure of the formed PLG-CA4 (Fig. 1B) was confirmed by <sup>1</sup>H NMR. Resonance peaks at δ 6.57 (k), 6.44 (j), 6.29 (i), 3.62 (h) and 4.02 (g) ppm were attributed to the presence of CA4. HPLC was applied to test the free CA4 content in the PLG-CA4 conjugates. As shown in Fig. 1C, no detectable free CA4 was found in the conjugates, suggesting that the purity of the obtained conjugates is high. No free CA4 exists in the obtained PLG-CA4 conjugates. The final PLG-CA4 conjugates had a CA4 drug loading content (DLC%) of 33.7 wt% as confirmed by UV-Vis spectrometry (Fig. 1D), indicating that the average number of CA4 moieties per polymer chain is 96.8.

The prepared PLG-CA4 conjugates formed spheres in mimic physiological conditions (PBS pH 7.4), with a diameter of 28.0 nm (TEM, Fig. S1) and  $D_h$  of 36.4 nm (DLS, Polydispersity: 0.249, Fig. 1E). We tested the *in vitro* release of CA4 from the conjugates in distilled water, PBS pH 7.4 and pH 5.5 (Fig. S2). The conjugates were found to be stable in distilled water, in which less than 10% was released in 48 h, whereas in PBS pH 7.4 and pH 5.5, the release of CA4 exhibited a pH-dependent release profile. The release rate of CA4 at pH 7.4 is faster than those at pH 5.5 and in distilled water. This phenomenon should be attributed to the nucleophilic attack of the hydroxyl or carboxylate ions on the carbonyl groups that are adjacent to CA4 moieties in the PBS pH 7.4 [59]. Only 15% of CA4 is released from PLG-CA4 in 10% BSA solution (Fig. S3) in

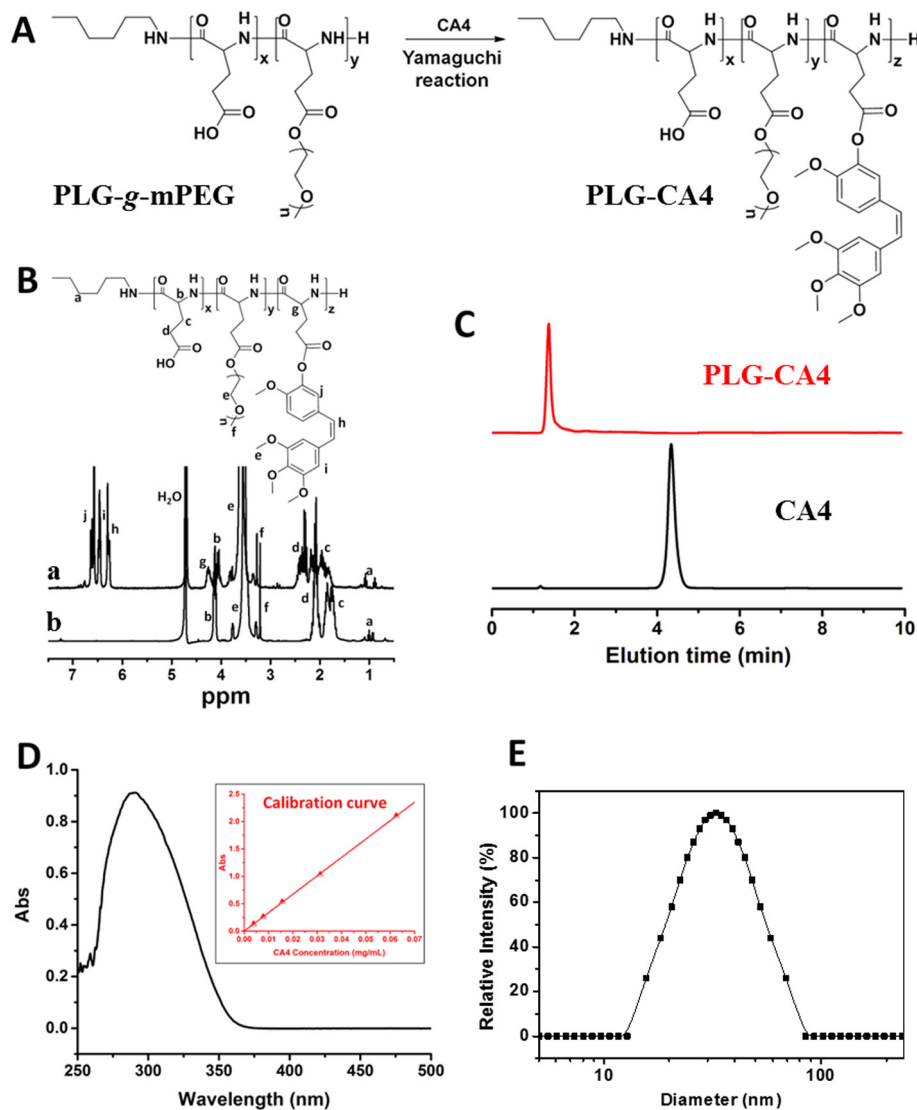


**Fig. 1.** Preparation and characterization of PLG-CA4: (A) Synthesis of PLG-CA4; (B) <sup>1</sup>H NMR spectra of PLG-CA4 (a) and PLG-g-mPEG (b); (C) HPLC curves of PLG-CA4 and free CA4; (D) UV-Vis spectrum of 0.25 mg/mL PLG-CA4 in DMF/H<sub>2</sub>O (v/v = 1/1). The absorbance peak of CA4 is at 290 nm. Insert is the calibration curve of CA4 absorbance vs. concentration. (E) Size distribution plots of PLG-CA4 obtained using DLS.

72 h, indicating that the PLG-CA4 is stable in the presence of plasma.

### 3.2. *In vitro* cytotoxicity tests

The *in vitro* tumor cell inhibition tests were conducted in C26 cells by MTT and CCK-8 assays. The C26 cell viability was measured by MTT assay. PLG-CA4 displayed a lower cytotoxicity towards C26 cells than CA4P at 24 h (Fig. S4A). However, at 48 h, PLG-CA4 exhibited similar cytotoxicity to the CA4P with IC<sub>50</sub> of 30.1 μg/mL for CA4P and 34.4 μg/mL for PLG-CA4 (Fig. S4B). The C26 cell growth was measured using CCK-8 assay. As shown in Fig. S5, CA4P and PLG-CA4 inhibited the growth of C26 cells in a similar manner at a concentration of 50 μg/mL on the basis of CA4. These indicated that the CA4P and PLG-CA4 had some inhibitory effect for the proliferation of cancer cells [60].

### 3.3. Pharmacokinetics

Wistar rats were administered PLG-CA4 or CA4P. Fig. 2A shows the total CA4 concentration in the plasma at different time inter-

vals. The distribution half-life time ( $t_{1/2\alpha}$ ) of PLG-CA4 was 2.49 h, and elimination half-life time ( $t_{1/2\beta}$ ) was 5.95 h. The AUC was calculated to be 2477.0 h × μg/mL. These are in contrast to CA4P that has a much shorter plasma life with  $t_{1/2\alpha}$  of 0.26 h,  $t_{1/2\beta}$  of 4.53 h and AUC of 45.6 h × μg/mL. This demonstrates that the period of time that PLG-CA4 is in the blood circulation can enhance accumulation and retention of CA4 in both the plasma and the tumor and result in prolonged vascular disruption.

### 3.4. *Ex vivo* RhoB-labeled PLG-CA4 fluorescence imaging

For biodistribution studies of PLG-CA4, imaging of the isolated visceral organs (heart, liver, spleen, lung, and kidney) and tumors at 4 and 24 h post-injection of RhoB-labeled PLG-CA4 were carried out in mice bearing C26 tumors. At 4 h post-injection, liver and lung showed strong Rhodamine B fluorescence. At 24 h post-injection, a stronger fluorescence signal was observed in tumor as compared with that of 4 h, and meanwhile liver, spleen and lung showed weaker fluorescence (Fig. 3). This suggested that the long blood circulation of PLG-CA4 had contributed to increase drug tumor accumulation by EPR effect.

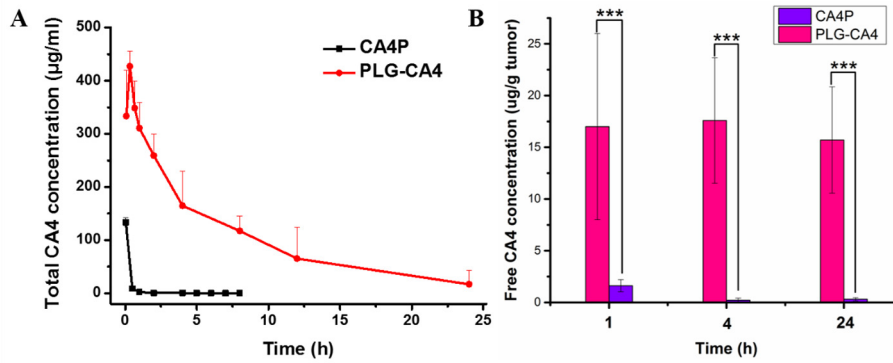


**Fig. 2.** Pharmacokinetics and tumor accumulation of PLG-CA4 and CA4P. (A) Time profiles of total CA4 concentration in the plasma after intravenous administration of PLG-CA4 or CA4P. Drugs were administered to healthy rats at a dose of 50 mg/kg based on CA4. Each group is expressed as mean  $\pm$  SD ( $n = 3$ ). (B) Free CA4 concentration in C26 tumors at 1 h, 4 h and 24 h following administration of CA4P and PLG-CA4, at CA4 dose of 50.0 mg/kg ( $n = 4$ , \*\*\*:  $p < 0.001$ ).

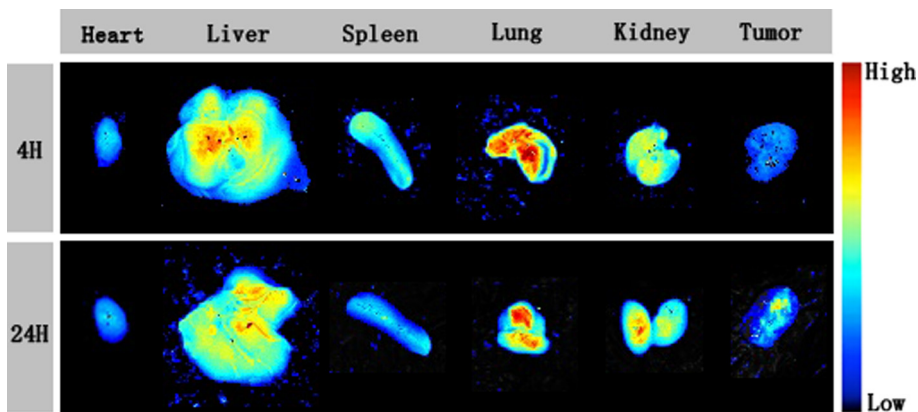


**Fig. 3.** Ex vivo Rhodamine B fluorescence images showing the biodistribution of RhoB-labeled PLG-CA4 in mice bearing C26 tumor at 4 and 24 h post-injection.

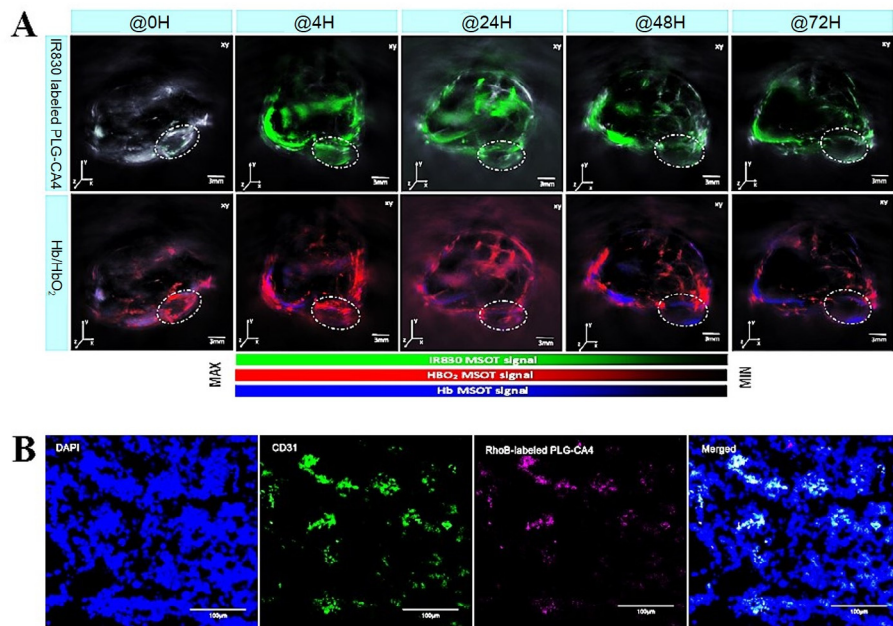


**Fig. 4.** Intra-tumor distribution of PLG-CA4. (A) Orthogonal views of MSOT images of C26 tumor-bearing mice at 4 h, 24 h, 48 h and 72 h after injection of IR830-labeled PLG-CA4 (with a CA4 dose of 50.0 mg/kg). The regions encircled with dashed white lines are tumor regions. Scale bar = 3 mm. (B) Immunofluorescence analysis of the C26 tumor at 24 h following injection with RhoB-labeled PLG-CA4. RhoB-labeled PLG-CA4 (red) are primarily located around the tumor blood vascular regions (green), which suggests that PLG-CA4 directs the conjugates to the vasculature within tumors. Scale bar = 100  $\mu$ m. (For interpretation of the references to colour in this figure legend, the reader is referred to the web version of this article.)

### 3.5. Free CA4 in tumor after the administration of CA4P or PLG-CA4

We compared the free CA4 concentrations from 1 to 24 h in tumors of the C26 mice after injection of CA4P and PLG-CA4 (Fig. 2B). Significant differences could be detected between the CA4P and PLG-CA4 groups. At 1 h, the free CA4 concentration of PLG-CA4 was 10-fold higher compared to that of the CA4P group. As time prolonged, free CA4 concentration in the CA4P group further decreased, to almost undetectable levels, whereas the free CA4 concentration in the PLG-CA4 group was constantly high. This reflected that PLG-CA4 accumulated in the tumor tissue and gradually released active CA4 through the hydrolysis of ester bonds catalyzed by acid or enzymes. The constantly high CA4 concentration inside tumors is expected to prolong the action time and strengthen the tumor therapeutic efficiency.

### 3.6. Intra-tumor distribution of PLG-CA4

Nanomedicine usually has low tissue penetration in solid tumors, which limits the efficacy of nanomedicine in most cases [40,61–64]. In order to study the tissue penetration of PLG-CA4 nanomedicine in solid tumor, the MSOT was applied to investigate the *in vivo* PLG-CA4 distribution and especially the location in relation to the tumor blood vessels. Oxy- and deoxyhemoglobin (HbO<sub>2</sub> and Hb) serve as endogenic probes for the MSOT test, and would direct the position of the blood vessels [64,65]. PLG-CA4 copolymers were labeled with IR830, a near-infrared probe with a maximum absorbance at 815 nm in water. As shown in Fig. 4A (The magnified area of interest was shown in Fig. S6), at 0 h, Hb/HbO<sub>2</sub> signals could be found in the tumor with neglectable IR830 signals. At 4 h after injection, IR830 signals could clearly be detected in the tumor, and were mainly distributed around the blood vessels, indicating the vascular-dependent distribution of the injected PLG-CA4 nanomedicine because of the low tissue penetration in solid tumor. Over time, fewer Hb/HbO<sub>2</sub> signals were detected inside the tumor, which indicated that many vessels inside the tumor were diminished and closed (Fig. S7).

We further confirmed the intra-tumor distribution of the PLG-CA4 by immunofluorescence staining. PLG-CA4 was labeled with RhoB, and the tumor tissues were analyzed at 24 h after injection. As shown in Fig. 4B, RhoB fluorescence for the RhoB-labeled PLG-CA4-treated group was primarily co-localized with the FITC fluorescence that detects vessels at 24 h, indicating that RhoB-labeled PLG-CA4 was localized in the vicinity or the endothelial cells of blood vessels. Consistent with the results obtained by MSOT, these results suggest that PLG-CA4 predominantly releases around tumor blood vessels, which is the target of active CA4. Considering the long retention time of PLG-CA4 inside the tumor tissue, the nanocarrier-loaded CA4 prodrug is expected to result in prolonged vascular disruption and significantly enhance tumor therapeutic efficiency.

Unfortunately, CA4P can not be detected by MSOT and immunofluorescence analysis, therefore it is impossible to observe the intra-tumor distribution of CA4P using these methods.

### 3.7. Pathological analysis after single administration of CA4P and PLG-CA4

H&E staining was used to evaluate the therapeutic effects of CA4P and PLG-CA4 treatment on tumor necrosis after single intravenous administration. As shown in Fig. S8, un-treated C26 tumor did not have necrosis. The H&E images from 4 to 72 h are summarized in Fig. 5(A–H). The necrotic area of the tumor showed increased neutrophil infiltration and fragmented nuclei of tumor cells (Fig. S9). Significant differences in the pathology could be detected between the CA4P (A–D) and PLG-CA4 (E–H) treatment

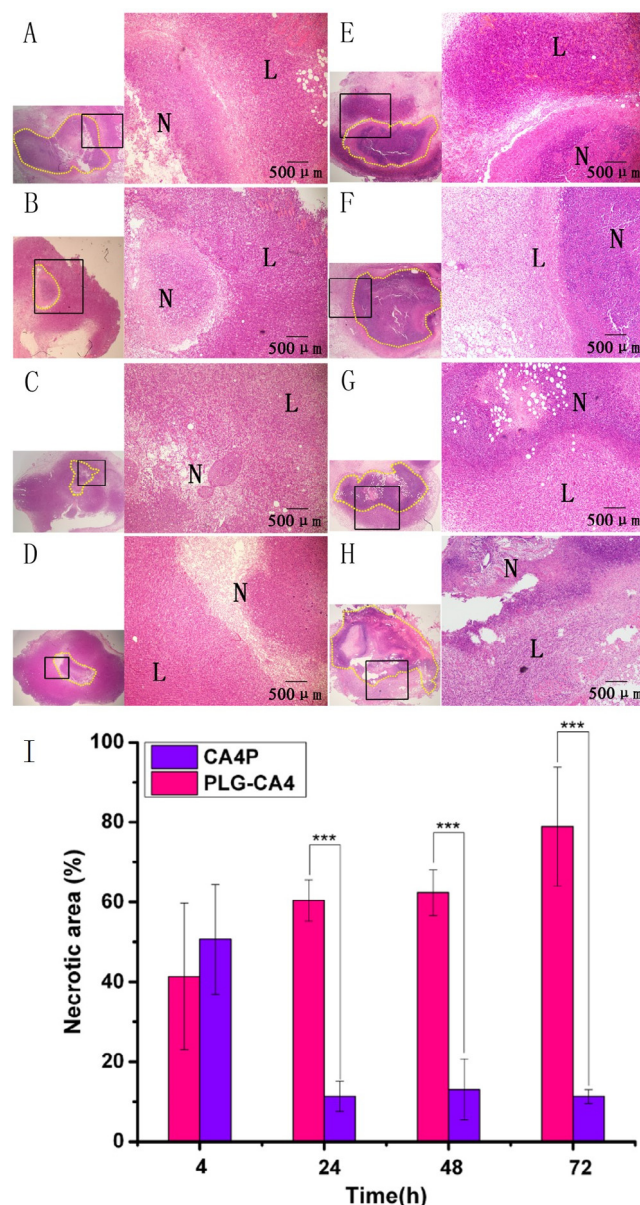


**Fig. 5.** Hematoxylin and eosin analysis of tumor tissues after treatment with CA4P (A–D) and PLG-CA4 (E–H) at a CA4 dose of 50.0 mg/kg. Per image: left, sections of whole tumor taken at  $\times 20$  magnification, right: magnification ( $\times 100$ ) of areas outlined at the left. L and N indicate the live and necrotic regions at various times after treatment: (A, E) 4 h, (B, F) 24 h, (C, G) 48 h and (D, H) 72 h. The yellow dashed circle indicates tumor necrotic tissue. I: Summarized percentage of necrotic areas across time ( $n = 4$ ,  $***p < 0.001$ ). (For interpretation of the references to colour in this figure legend, the reader is referred to the web version of this article.)

groups. At 4 h, both treatment with CA4P and treatment with PLG-CA4 resulted in large areas of necrosis (Fig. 5I). The necrotic rate of for the CA4P group was  $41.4 \pm 18.3\%$ , whereas for the PLG-CA4 group it was  $50.7 \pm 13.8\%$ . However, rapid tumor relapse occurred in the CA4P group over time, and after 24 h the necrotic areas represented only 10% because the C26 tumor continued to grow vigorously and laid down new live tumor tissues after CA4P treatment. The PLG-CA4 group showed continued tumor regression during the observation period, and the necrotic areas were still over  $60 \pm 5.1\%$  and even  $78.9 \pm 14.9\%$  at 72 h. These results showed a major advantage of PLG-CA4 over CA4P, and support the hypothesis that long-term and a constant high CA4 concentration around tumor vessels would result in sustained tumor blood deprivation and greater tumor regression.

Treatment with PLG-CA4 resulted in more profound tumor necrosis as compared to treatment with CA4P. As to our understanding, the tumor cells take advantage of being in proximity of normal tissue vessels from which they can get sufficient nutrients to survive. This may result in tumor relapse even when CA4P is used to block the tumor blood vessels. Therefore, we analyzed the necrosis status of cells nearby and surrounding normal tissues. As shown in Fig. S10, tumor cells near the muscle tissue were still alive in the CA4P treatment group, whereas those in the PLG-CA4 treatment group were almost necrotic. This result further confirmed the advantage of the use of PLG-CA4 over CA4P, and may in part explain the continuous inhibitory effect of PLG-CA4 treatment on tumor growth.

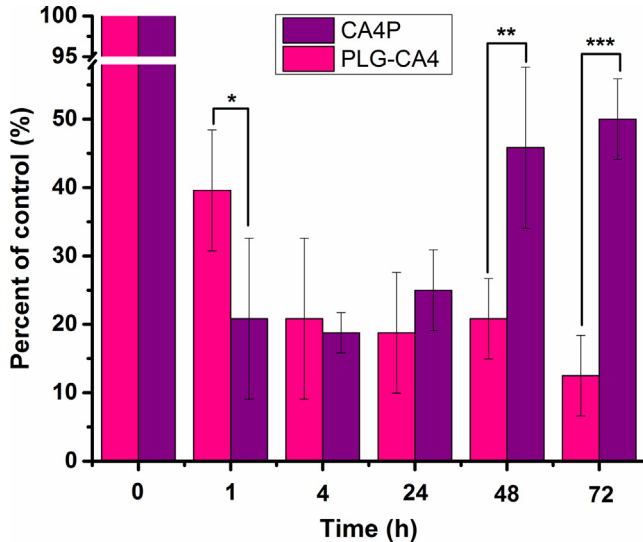


Fig. 6. Tumor vessel density: immunofluorescence assay for CD31 was performed to analyze whole tumor vessel density ( $n = 4$ ,  $p < 0.05$ ,  $**p < 0.01$ ,  $***p < 0.001$ ).

Next, we analyzed the vessel density of the tumor after treatment with CA4P and PLG-CA4 (Fig. 6). The vessel numbers in the CA4P treatment group quickly decreased within 1 h after start of the treatment to about 21% as compared to the control group, which was 100%. They subsequently recovered to 25% in 24 h, whereas the PLG-CA4 group showed continued vessel inhibition along the 72 h observation, with 21% of vessel numbers at 4 h and 13% at 72 h. These results confirmed that the small molecular prodrug CA4P disrupts tumor blood vessels for a relatively short period of time, whereas the polymeric prodrug PLG-CA4 destroys tumor blood vessels over a longer time period. These results also explained why the tumor relapsed at 24 h after single CA4P administration, whereas no relapse occurred in 72 h after PLG-CA4 treatment.

In order to investigate whether normal organ blood vessels were damaged after the administration of PLG-CA4, we studied the normal organs using H&E stain. As shown in Fig. S11, the normal organ blood vessels from heart, liver, spleen, lung or kidney were not damaged with the treatment of PLG-CA4 at a dose of 50 mg/kg (on the basis of CA4). This indicates that PLG-CA4 has not damaged normal organ blood vessels.

### 3.8. In vivo tumor therapy

Lastly, we compared the therapeutic efficacy of the two groups on Balb/C mice bearing C26 tumors. Once the tumor volumes reached approximately 100 mm<sup>3</sup>, saline, CA4P or PLG-CA4 were administered on the 1st, 5th and 9th day. We found that PLG-CA4 was significantly more effective at inhibiting tumor growth compared to CA4P treatment groups at equal dose (Fig. 7A). On day 11, most of the tumor tissue appeared to be nearly completely diminished in the PLG-CA4 group (Fig. 7B). On the 17th day, PLG-CA4 and CA4P treatment resulted in tumor suppression rates of 74% and 24%, respectively (Fig. 7C). Three injections of CA4P (50 mg/kg based on CA4) turned out to be an ineffective treatment for controlling the tumor growth of C26 tumors. This may be

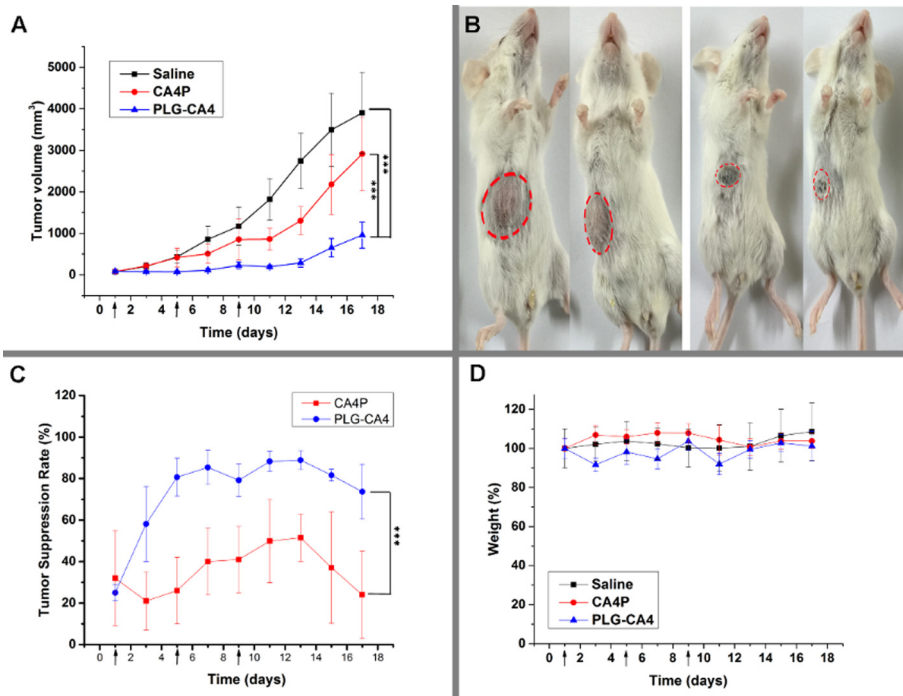
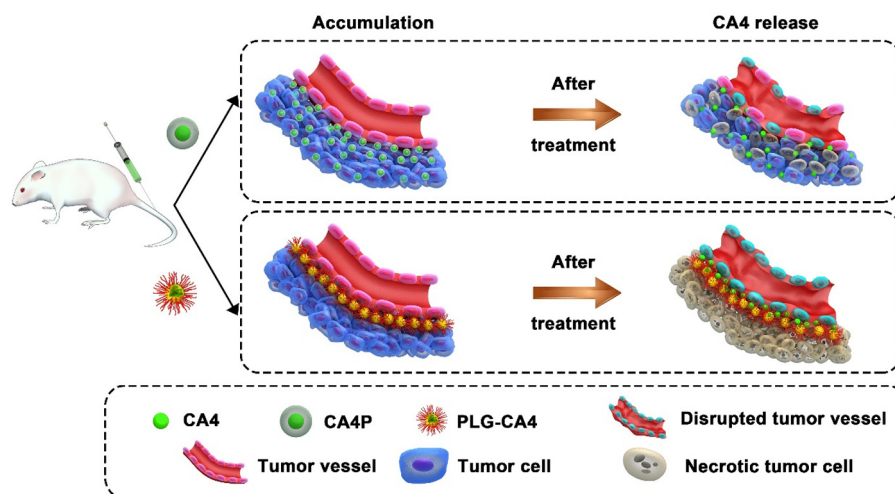


Fig. 7. In vivo tumor therapy results. (A) C26 tumor volumes after injection with saline, PLG-CA4 and CA4P on days 1, 5 and 9. (B) Images of C26 tumors on day 11; mice on the left were treated with CA4P and mice on the right were treated with PLG-CA4. The red dashed circle shows the tumor region. (C) C26 tumor suppression rate after injection with PLG-CA4 or CA4P on days 1, 5 and 9. (D) Body weight changes ( $n = 6$ ,  $***p < 0.001$ ).



**Fig. 8.** Mechanism of PLG-CA4 and CA4P for solid tumor treatment. After tail vein injection, PLG-CA4 nanomedicine arrive and arrest around tumor vessels, CA4 is gradually released and acts constantly on endothelial cells, resulting in endothelial cells deformation, diminished blood flow, oxygen and nutrient deprivation and widespread tumor cell necrosis. CA4P arrives and arrests around tumor vessels for a short period of time resulting in tumor cells that are alive and less necrotic than when treated with PLG-CA4.

explained by the short-lived and reversible activity of free CA4. Treatment with PLG-CA4 (50 mg/kg based on CA4) resulted in much better inhibition of tumor growth compared to CA4P, confirming that a high and constant CA4 concentration around tumor vessels are necessary for controlling tumor growth. In addition, no obvious body weight loss was observed in both groups (Fig. 7D), suggesting the low side effects of the treatments.

The above results showed the superiority of the PLG-CA4 conjugates nanomedicine over CA4P on solid tumor therapy. As shown in Fig. 8, in our opinion the advantages can be summarized as follows: 1) PLG-CA4 has a long *in vivo* plasma retention time, and accumulates in the tumor tissue due to the befitting size and EPR effect, 2) active CA4 is gradually released inside the tumor and maintains high and constant active drug concentration over a long period of time, 3) these nano-sized drugs are primarily located around tumor vessels due to the high interstitial pressure and inefficient diffusion, making the active drugs arrested adjuvant action target and 4) PLG-CA4 treatment results in markedly enhanced tumor therapy efficiency as compared to CA4P treatment.

#### 4. Conclusions

In summary, we developed a novel nanosized polymeric CA4 prodrug, PLG-CA4, and determined its therapeutic efficiency and benefits on solid tumor therapy. PLG-CA4 showed longer plasma retention than CA4P. In solid tumor tissue, the accumulated PLG-CA4 gradually released free CA4, and maintained constant high CA4 concentration inside the tumor. The distribution of PLG-CA4 in tumors was highly vascular-dependent, and mainly arrested around tumor vessels. After single administration, PLG-CA4 treatment resulted in  $78.9 \pm 14.9\%$  necrotic areas in tumor tissue, and this effect lasted for over 72 h. C26 tumors treated with PLG-CA4 resulted in significantly higher anticancer effects as compared to treatment with CA4P. The results in this study suggested the prominent advantages of VDA-nanomedicine over small molecular VDA.

#### Acknowledgments

This research was financially supported by National Natural Science Foundation of China (Projects 51473029, 51233004, 51390484, 51673189, 51373168, 51528303 and 51403204) and

the Chinese Academy of Sciences Youth Innovation Promotion Association.

#### Appendix A. Supplementary data

Supplementary material (TEM image of PLG-CA4, *in vitro* release of CA4 from PLG-CA4, viability and growth of C26 tumor cells after incubation with CA4P or PLG-CA4, Magnified area of interest of orthogonal views of MSOT images, H&E staining of tumor tissues without treatment, H&E staining of normal organs (heart, liver, spleen, lung and kidney) slices with the treatment of PLG-CA4, MSOT signal of IR830-labeled PLG-CA4 and Hb/HbO<sub>2</sub> in C26 tumor tissue, neutrophil infiltration and fragmented nuclei of tumor cells in treated tumor, and hematoxylin and eosin staining of muscle tissue adjacent to tumor tissue), is available in the online version, at <http://dx.doi.org/10.1016/j.actbio.2017.02.001>.

#### References

- [1] K. Hida, N. Maishi, C. Torii, Y. Hida, Tumor angiogenesis—characteristics of tumor endothelial cells, *Int. J. Clin. Oncol.* 21 (2) (2016) 206–212.
- [2] L.J. Rich, M. Seshadri, Photoacoustic imaging of vascular hemodynamics: validation with blood oxygenation level-dependent MR imaging, *Radiology* 275 (1) (2015) 110–118.
- [3] T.E. Strecker, S.O. Odutola, R. Lopez, M.S. Cooper, J.K. Tidmore, A.K. Charlton-Sevcik, L. Li, M.T. MacDonough, M.B. Hadimani, A. Ghatak, L. Liu, D.J. Chaplin, R. P. Mason, K.G. Pinney, M.L. Trawick, The vascular disrupting activity of OXi8006 in endothelial cells and its phosphate prodrug OXi8007 in breast tumor xenografts, *Cancer Lett.* 369 (1) (2015) 229–241.
- [4] J. Folkman, Tumor angiogenesis: therapeutic implications, *N. Engl. J. Med.* 285 (21) (1971) 1182–1186.
- [5] J. Folkman, How is blood vessel growth regulated in normal and neoplastic tissue? G.H.A. Clowes memorial Award lecture, *Cancer Res.* 46 (2) (1986) 467–473.
- [6] P. Hahnfeldt, D. Panigrahy, J. Folkman, L. Hlatky, Tumor development under angiogenic signaling: a dynamical theory of tumor growth, treatment response, and postvascular dormancy, *Cancer Res.* 59 (19) (1999) 4770–4775.
- [7] G. Dougherty, D. Chaplin, T. Meyer, *Vascular Disruptive Agents for the Treatment of Cancer*, Springer, New York, 2010.
- [8] R.H. Zha, S. Sur, J. Boekhoven, H.Y. Shi, M. Zhang, S.I. Stupp, Supramolecular assembly of multifunctional mabpin-mimetic nanostructures as a potent peptide-based angiogenesis inhibitor, *Acta Biomater.* 12 (2015) 1–10.
- [9] D.W. Siemann, D.J. Chaplin, M.R. Horsman, Vascular-targeting therapies for treatment of malignant disease, *Cancer* 100 (12) (2004) 2491–2499.
- [10] R.P. Mason, D. Zhao, L. Liu, M.L. Trawick, K.G. Pinney, A perspective on vascular disrupting agents that interact with tubulin: preclinical tumor imaging and biological assessment, *Integr. Biol.* 3 (4) (2011) 375–387.
- [11] W. Song, Z. Tang, D. Zhang, M. Li, J. Gu, X. Chen, A cooperative polymeric platform for tumor-targeted drug delivery, *Chem. Sci.* 7 (1) (2016) 728–736.

- [12] E. Hamel, C.M. Lin, Interactions of combretastatin, a new plant-derived antimetabolic agent, with tubulin, *Biochem. Pharmacol.* 32 (24) (1983) 3864–3867.
- [13] C. Kanthou, G.M. Tozer, The tumor vascular targeting agent combretastatin A-4-phosphate induces reorganization of the actin cytoskeleton and early membrane blebbing in human endothelial cells, *Blood* 99 (6) (2002) 2060–2069.
- [14] G.M. Tozer, V.E. Prise, J. Wilson, R.J. Locke, B. Vojnovic, M.R.L. Stratford, M.F. Dennis, D.J. Chaplin, Combretastatin A-4 phosphate as a tumor vascular-targeting agent: early effects in tumors and normal tissues, *Cancer Res.* 59 (7) (1999) 1626–1634.
- [15] G.M. Tozer, V.E. Prise, J. Wilson, M. Cemazar, S.Q. Shan, M.W. Dewhurst, P.R. Barber, B. Vojnovic, D.J. Chaplin, Mechanisms associated with tumor vascular shut-down induced by combretastatin A-4 phosphate: intravital microscopy and measurement of vascular permeability, *Cancer Res.* 61 (17) (2001) 6413–6422.
- [16] S.M. Galbraith, D.J. Chaplin, F. Lee, M.R.L. Stratford, R.J. Locke, B. Vojnovic, G.M. Tozer, Effects of combretastatin A4 phosphate on endothelial cell morphology in vitro and relationship to tumor vascular targeting activity in vivo, *Anticancer Res.* 21 (1A) (2001) 93–102.
- [17] L. Vincent, P. Kermani, L.M. Young, J. Cheng, F. Zhang, K. Shido, G. Lam, H. Bompais-Vincent, Z.P. Zhu, D.J. Hicklin, P. Bohlen, D.J. Chaplin, C. May, S. Rafii, Combretastatin A4 phosphate induces rapid regression of tumor neovessels and growth through interference with vascular endothelial-cadherin signaling, *J. Clin. Invest.* 115 (11) (2005) 2992–3006.
- [18] S.X. Cai, Small molecule vascular disrupting agents: potential new drugs for cancer treatment, *Recent Pat. Anticancer Drug Discovery* 2 (1) (2007) 79–101.
- [19] M.A. Marx, Small-molecule, tubulin-binding compounds as vascular targeting agents, *Expert Opin. Ther. Pat.* 12 (6) (2002) 769–776.
- [20] C.M.L. West, P. Price, Combretastatin A4 phosphate, *Anticancer Drugs* 15 (3) (2004) 179–187.
- [21] G.R. Pettit, C. Temple, V.L. Narayanan, R. Varma, M.J. Simpson, M.R. Boyd, G.A. Rener, N. Bansal, Antineoplastic agents-322 – Synthesis of combretastatin a-4 prodrugs, *Anti-Cancer Drug Des.* 10 (4) (1995) 299–309.
- [22] The more details about clinical studies of CA4P should be found in the website of “Clinical Trials”. <<https://clinicaltrials.gov/ct2/results?term=CA4P>>.
- [23] A. Dowlati, K. Robertson, M. Cooney, W.P. Petros, M. Stratford, J. Jesberger, N. Rafie, B. Overmoyer, V. Makkar, B. Stambler, A. Taylor, J. Waas, J.S. Lewin, K.R. McCrae, S.C. Remick, A phase I pharmacokinetic and translational study of the novel vascular targeting agent combretastatin A-4 phosphate on a single-dose intravenous schedule in patients with advanced cancer, *Cancer Res.* 62 (12) (2002) 3408–3416.
- [24] J.P. Stevenson, M. Rosen, W.J. Sun, M. Gallagher, D.G. Haller, D. Vaughn, B. Giantonio, R. Zimmer, W.P. Petros, M. Stratford, D. Chaplin, S.L. Young, M. Schnall, P.J. O'Dwyer, Phase I trial of the antivascular agent combretastatin A4 phosphate on a 5-day schedule to patients with cancer: magnetic resonance imaging evidence for altered tumor blood flow, *J. Clin. Oncol.* 21 (23) (2003) 4428–4438.
- [25] G.J.S. Rustin, S.M. Galbraith, H. Anderson, M. Stratford, L.K. Folkes, L. Sena, L. Gumbrell, P.M. Price, Phase I clinical trial of weekly combretastatin A4 phosphate: clinical and pharmacokinetic results, *J. Clin. Oncol.* 21 (15) (2003) 2815–2822.
- [26] C.J. Mooney, G. Nagaiah, P.F. Fu, J.K. Wasman, M.M. Cooney, P.S. Savvides, J.A. Bokar, A. Dowlati, D. Wang, S.S. Agarwala, S.M. Flick, P.H. Hartman, J.D. Ortiz, P. N. Lavertu, S.C. Remick, A phase II trial of fosbretabulin in advanced anaplastic thyroid carcinoma and correlation of baseline serum-soluble intracellular adhesion molecule-1 with outcome, *Thyroid* 19 (3) (2009) 233–240.
- [27] C.M. Lin, H.H. Ho, G.R. Pettit, E. Hamel, Antimetabolic natural-products combretastatin-a-4 and combretastatin-a-2 – studies on the mechanism of their inhibition of the binding of colchicine to tubulin, *Biochemistry* 28 (17) (1989) 6984–6991.
- [28] S.A. Hill, G. Tozer, G.R. Pettit, D.J. Chaplin, Preclinical evaluation of the antitumor activity of the novel vascular targeting agent Oxi 4503, *Anticancer Res.* 22 (3) (2001) 1453–1458.
- [29] K. Grosios, S. Holwell, A.T. McGown, G. Pettit, M. Bibby, In vivo and in vitro evaluation of combretastatin A-4 and its sodium phosphate prodrug, *Br. J. Cancer* 81 (8) (1999) 1318.
- [30] D. Peer, J.M. Karp, S. Hong, O.C. FaroKHzad, R. Margalit, R. Langer, Nanocarriers as an emerging platform for cancer therapy, *Nat. Nanotechnol.* 2 (12) (2007) 751–760.
- [31] H. Maeda, Macromolecular therapeutics in cancer treatment: the EPR effect and beyond, *J. Control. Release* 164 (2) (2012) 138–144.
- [32] Y.Z. Min, J.M. Caster, M.J. Eblan, A.Z. Wang, Clinical translation of nanomedicine, *Chem. Rev.* 115 (19) (2015) 11147–11190.
- [33] W.T. Song, Z.H. Tang, D.W. Zhang, Y. Zhang, H.Y. Yu, M.Q. Li, S.X. Lv, H. Sun, M. X. Deng, X.S. Chen, Anti-tumor efficacy of c(RGDfK)-decorated polypeptide-based micelles co-loaded with docetaxel and cisplatin, *Biomaterials* 35 (9) (2014) 3005–3014.
- [34] H. Xu, D. Yang, C. Cai, J. Gou, Y. Zhang, L. Wang, H. Zhong, X. Tang, Dual-responsive mPEG-PLGA-PGLu hybrid-core nanoparticles with a high drug loading to reverse the multidrug resistance of breast cancer: an in vitro and in vivo evaluation, *Acta Biomater.* 16 (2015) 156–168.
- [35] Z. Tang, C. He, H. Tian, J. Ding, B.S. Hsiao, B. Chu, X. Chen, Polymeric nanostructured materials for biomedical applications, *Prog. Polym. Sci.* 60 (2016) 86–128.
- [36] M.M. Sheno, I. Iltis, J. Choi, N.A. Koonce, G.J. Metzger, R.J. Griffin, J.C. Bischof, Nanoparticle delivered vascular disrupting agents (VDAs): use of TNF-alpha conjugated gold nanoparticles for multimodal cancer therapy, *Mol. Pharm.* 10 (5) (2013) 1683–1694.
- [37] S. Sengupta, D. Eavarone, I. Capila, G.L. Zhao, N. Watson, T. Kiziltepe, R. Sasisekharan, Temporal targeting of tumour cells and neovasculature with a nanoscale delivery system, *Nature* 436 (7050) (2005) 568–572.
- [38] Y.G. Wang, T.Y. Yang, X. Wang, W.B. Dai, J.C. Wang, X.A. Zhang, Z.Q. Li, Q.A. Zhang, Materializing sequential killing of tumor vasculature and tumor cells via targeted polymeric micelle system, *J. Control. Release* 149 (3) (2011) 299–306.
- [39] W.T. Song, Z.H. Tang, D.W. Zhang, H.Y. Yu, X.S. Chen, Coadministration of vascular disrupting agents and nanomedicines to eradicate tumors from peripheral and central regions, *Small* 11 (31) (2015) 3755–3761.
- [40] H. Lee, H. Fonge, B. Hoang, R.M. Reilly, C. Allen, The effects of particle size and molecular targeting on the intratumoral and subcellular distribution of polymeric nanoparticles, *Mol. Pharm.* 7 (4) (2010) 1195–1208.
- [41] S.D. Perrault, C. Walkey, T. Jennings, H.C. Fischer, W.C.W. Chan, Mediating tumor targeting efficiency of nanoparticles through design, *Nano Lett.* 9 (5) (2009) 1909–1915.
- [42] L. Tang, X.J. Yang, Q. Yin, K.M. Cai, H. Wang, I. Chaudhury, C. Yao, Q. Zhou, M. Kwon, J.A. Hartman, I.T. Dobrucki, L.W. Dobrucki, L.B. Borst, S. Lezmig, W.G. Helferich, A.L. Ferguson, T.M. Fan, J.J. Cheng, Investigating the optimal size of anticancer nanomedicine, *Proc. Natl. Acad. Sci. U.S.A.* 111 (43) (2014) 15344–15349.
- [43] W. Song, Z. Tang, N. Shen, H. Yu, Y. Jia, D. Zhang, J. Jiang, C. He, H. Tian, X. Chen, Combining disulfiram and poly(L-glutamic acid)-cisplatin conjugates for combating cisplatin resistance, *J. Control. Release* 231 (2016) 94–102.
- [44] H.Y. Yu, Z.H. Tang, D.W. Zhang, W.T. Song, Y. Zhanga, Y. Yang, Z. Ahmad, X.S. Chen, Pharmacokinetics, biodistribution and in vivo efficacy of cisplatin loaded poly(L-glutamic acid)-g-methoxy poly(ethylene glycol) complex nanoparticles for tumor therapy, *J. Control. Release* 205 (2015) 89–97.
- [45] C. Shi, H. Yu, D. Sun, L. Ma, Z. Tang, Q. Xiao, X. Chen, Cisplatin-loaded polymeric nanoparticles: Characterization and potential exploitation for the treatment of non-small cell lung carcinoma, *Acta Biomater.* 18 (2015) 68–76.
- [46] Y. Niu, W. Song, D. Zhang, Z. Tang, M. Deng, X. Chen, Functional computer-to-plate near-infrared absorbers as highly efficient photoacoustic dyes, *Acta Biomater.* 43 (2016) 262–268.
- [47] P. Bono, V.-M. Wasenius, P. Heikkilä, J. Lundin, D.G. Jackson, H. Joensuu, High LYVE-1-Positive lymphatic vessel numbers are associated with poor outcome in breast cancer, *Clin. Cancer Res.* 10 (21) (2004) 7144–7149.
- [48] A. Abramsson, Ö. Berlin, H. Papayan, D. Paulin, M. Shani, C. Betsholtz, Analysis of mural cell recruitment to tumor vessels, *Circulation* 105 (1) (2002) 112–117.
- [49] J. Drevs, I. Hofmann, H. Hugschmidt, C. Wittig, H. Madjar, M. Müller, J. Wood, G. Martiny-Baron, C. Unger, D. Marmé, Effects of PTK787/ZK 222584, a specific inhibitor of vascular endothelial growth factor receptor tyrosine kinases, on primary tumor, metastasis, vessel density, and blood flow in a murine renal cell carcinoma model, *Cancer Res.* 60 (17) (2000) 4819–4824.
- [50] C. He, X. Zhuang, Z. Tang, H. Tian, X. Chen, Stimuli-sensitive synthetic polypeptide-based materials for drug and gene delivery, *Adv. Healthcare Mater.* 1 (1) (2012) 48–78.
- [51] L.S. Nair, C.T. Laurencin, Polymers as biomaterials for tissue engineering and controlled drug delivery, *Adv. Biochem. Eng. Biotechnol.* 102 (2006) 47–90.
- [52] W. Song, Z. Tang, D. Zhang, Y. Zhang, H. Yu, M. Li, S. Lv, H. Sun, M. Deng, X. Chen, Anti-tumor efficacy of c(RGDfK)-decorated polypeptide-based micelles co-loaded with docetaxel and cisplatin, *Biomaterials* 35 (9) (2014) 3005–3014.
- [53] W. Song, Z. Tang, M. Li, S. Lv, H. Sun, M. Deng, H. Liu, X. Chen, Polypeptide-based combination of paclitaxel and cisplatin for enhanced chemotherapy efficacy and reduced side-effects, *Acta Biomater.* 10 (3) (2014) 1392–1402.
- [54] Z. Ahmad, S. Lv, Z. Tang, A. Shah, X. Chen, Methoxy poly(ethylene glycol)-block-poly(L-glutamic acid)-graft-6-(2-nitroimidazole) hexyl amine nanoparticles for potential hypoxia-responsive delivery of doxorubicin, *J. Biomater. Sci. Polym. Ed.* 27 (1) (2016) 40–54.
- [55] F. Koizumi, M. Kitagawa, T. Negishi, T. Onda, S. Matsumoto, T. Hamaguchi, Y. Matsumura, Novel SN-38-incorporating polymeric micelles, NK012, eradicate vascular endothelial growth factor-secreting bulky tumors, *Cancer Res.* 66 (20) (2006) 10048–10056.
- [56] C. Li, Poly(L-glutamic acid)-anticancer drug conjugates, *Adv. Drug Deliv. Rev.* 54 (5) (2002) 695–713.
- [57] J. Nemunaitis, C. Cunningham, N. Senzer, M. Gray, F. Oldham, J. Phippen, R. Mennel, A. Eisenfeld, Phase I study of CT-2103, a polymer-conjugated paclitaxel, and carboplatin in patients with advanced solid tumors, *Cancer Invest.* 23 (8) (2005) 671–676.
- [58] H. Yu, Z. Tang, M. Li, W. Song, D. Zhang, Y. Zhang, Y. Yang, H. Sun, M. Deng, X. Chen, Cisplatin loaded poly(L-glutamic acid)-g-methoxy poly(ethylene glycol) complex nanoparticles for potential cancer therapy: preparation, in vitro and in vivo evaluation, *J. Biomed. Nanotechnol.* 12 (1) (2016) 69–78.
- [59] E. Gaetjens, H. Morawetz, Intramolecular carboxylate attack on ester groups. The hydrolysis of substituted phenyl acid succinates and phenyl acid glutarates I, *J. Am. Chem. Soc.* 82 (20) (1960) 5328–5335.
- [60] G.G. Dark, S.A. Hill, V.E. Prise, G.M. Tozer, G.R. Pettit, D.J. Chaplin, Combretastatin A-4, an agent that displays potent and selective toxicity toward tumor vasculature, *Cancer Res.* 57 (10) (1997) 1829–1834.

- [61] Y.H. Bae, K. Park, Targeted drug delivery to tumors: myths, reality and possibility, *J. Control. Release* 153 (3) (2011) 198–205.
- [62] A.I. Minchinton, I.F. Tannock, Drug penetration in solid tumours, *Nat. Rev. Cancer* 6 (8) (2006) 583–592.
- [63] Q.H. Sun, X.R. Sun, X.P. Ma, Z.X. Zhou, E.L. Jin, B. Zhang, Y.Q. Shen, E.A. Van Kirk, W.J. Murdoch, J.R. Lott, T.P. Lodge, M. Radosz, Y.L. Zhao, Integration of nanoassembly functions for an effective delivery cascade for cancer drugs, *Adv. Mater.* 26 (45) (2014) 7615–7621.
- [64] W. Song, Z. Tang, D. Zhang, X. Wen, S. Lv, Z. Liu, M. Deng, X. Chen, Solid tumor therapy using a cannon and pawn combination strategy, *Theranostics* 6 (7) (2016) 1023–1030.
- [65] W. Song, Z. Tang, D. Zhang, N. Burton, W. Driessen, X. Chen, Comprehensive studies of pharmacokinetics and biodistribution of indocyanine green and liposomal indocyanine green by multispectral optoacoustic tomography, *RSC Adv.* 5 (5) (2015) 3807–3813.